이학석사 학위논문

The structural or electrical properties change of $Ba_{1-x}K_xBiO_3$ films via controlling laser fluence and buffer layer by using Pulsed Laser Deposition

펄스레이저 증착에서 레이저 세기속 조절과 완충 층 사용을 통한 $Ba_{1-x}K_xBiO_3$ 박막의 구조적 또는 전기적 물성 연구

2016 년 12월

서울대학교 대학원

물리천문학부

이 호 동

The structural or electrical properties change of $Ba_{1-x}K_xBiO_3$ films via controlling laser fluence and buffer layer by using Pulsed Laser Deposition

펄스레이저 증착에서 레이저 세기속 조절과 완충 층 사용을 통한 $Ba_{1-x}K_xBiO_3$ 박막의 구조적 또는 전기적 물성 연구

지도 교수 노 태 원

이 논문을 이학석사 학위논문으로 제출함

2016 년 12월

서울대학교 대학원

물리천문학부

이 호 동

이호동의 이학석사 학위논문을 인준함

2016 년 12월

위 원 장 _____

부위원장 _____

위 원 _____

Abstract

We investigated growth control of superconducting properties of BKBO films, by varying laser fluence using pulsed laser deposition technique. As cation stoichiometry, especially potassium concentration in BKBO films, was sensitively changed with laser fluence, we were able to precisely control T_c of BKBO films. Following the trend of the bulk phase diagram, T_c showed the highest value of 24.5 ± 0.5 K at the optimal stoichiometry.

Furthermore, we obtained a partially tensile-strained BKBO film with $BaBiO_3$ buffer layer, and a well tensile-strained BKBO film with a $BaCeO_3$ / $BaZrO_3$ double buffer layer. In the both case, we observed sharp full-width-half-maximum of the BKBO (002) reflection rocking curve in X-ray diffractometer measurement, which shows the potential for BKBO films with few crystallographic defects by reducing the lattice mismatch with various buffer layer.

Preface

$Ba_{1-x}K_xBiO_3$ (BKBO) is a well-known high-T_c oxide superconductor with a transition temperature of 31 K highest among oxides except cuprates. As holes are doped into a parent compound $BaBiO_3$, a charge density wave insulator, a complicated phase diagram, accompanied with structural transitions, has been reported. Intriguingly, superconductivity only emerges at a large potassium doping ($0.37 < x < 0.55$), Detailed studies on the phase diagram of BKBO have often been hindered due to difficulty in sample growth, where physical properties are subject to change by small differences in stoichiometry that can hardly be controlled in bulk.

In this study, we investigated growth control of superconducting properties of BKBO films, by varying laser fluence using pulsed laser deposition technique. Even though laser fluence is an essential factor for controlling cation stoichiometry in oxide film growth. [15-17], its effect on superconducting BKBO films has been seldom studied. Especially, a subtle compositional deviation from the stoichiometric BKBO film can result in destroying its superconducting behavior. Therefore, it is necessary to devise comprehensive guidelines for manufacturing high-quality BKBO, by optimizing laser fluence.

Furthermore, it also has not been studied on surface morphology and crystal quality of BKBO films in detail. Failure to obtain a flat and homogeneous BKBO surface is associated with the lattice mismatch between the substrate and film [22-23]. We assumed that the lattice

mismatch leads to the lattice imperfections in the film, which can harm the superconducting transition property of BKBO films, and hamper future research on BKBO films, such as Angle-resolved photoemission spectroscopy (ARPES) measurement, fabricating a superlattice, or liquid gating experiment. Therefore, it is important to find a way to avoid the large lattice mismatch between the film and substrate in order to enhance crystal quality and flatness of the BKBO film.

In chapter 3, we studied the effect of laser fluence on the superconductivity of BKBO films grown by PLD. We found that increasing the laser fluence resulted in contraction of lattice parameters, accompanying large variations in the cation stoichiometry. In particular, K concentration could be sensitively adjusted with laser fluence, which allowed the precise control of superconducting properties of the BKBO films. Furthermore, T_c of the BKBO films followed the trend of the bulk phase diagram with variation of laser fluence.

In chapter 4, we studied the effect of various buffer layers, which could provide the strain on BKBO films with a relatively small lattice mismatch. We obtained a partially tensile-strained BKBO film with $BaBiO_3$ buffer layer, and a well tensile-strained BKBO film with a $BaCeO_3$ / $BaZrO_3$ double buffer layer. In the both case, we observed sharp full-width-half-maximum (FWHM) of the (002) reflection rocking curve (0.07 deg.) of the films in X-ray diffractometer measurement, which were narrower than the BKBO films without the buffer layer by more than 10

times. This result shows that the high-quality BKBO films are possible by controlling the lattice mismatch with various buffer layer.

Contents

List of Figures

1. Introduction

1.1. Backgrounds

$BaBiO_3$ (BBO), which is the mother material of high-Tc superconducting $BaPb_{1-x}Bi_xO_3$ (BPBO) and $Ba_{1-x}K_xBiO_3$ (BKBO), shows the insulating behavior. This cannot be explained with a uniform Bi^{4+} distribution in BBO, because a half-filled $6s^1$ band should result in a metallic behavior of BBO. The charge disproportion, where the Bi charges are alternately ordered as Bi^{3+} and Bi^{5+}, makes BBO have special properties like octahedral breathing distortion, which results in lattice doubling.

The research on hole-doped BBO, such as BPBO and BKBO, was led by the attempts for searching an insulator-metal transition in BBO material. Especially, BKBO has attracted research attention for its high superconducting transition temperature, T_c, of ~31 K, which is the highest among non-cuprate oxide superconductors [1-3]. BKBO has a simple perovskite structure, composed of Bi-O_6 octahedra, with Bi ions at the perovskite *B*-site. Both material have a complex phase diagram with varying doping ratio [4-6]. For BKBO, for example, a wide semiconducting region appears for $0.1 < x < 0.3$ owing to bipolaronic hole trapping [7], and metallicity and superconductivity emerge simultaneously and T_c reaches its highest value of ~31 K around $x = 0.35$. Also, the structural phase transition from the cubic at high

temperature to the tetragonal in its superconducting region suggests that there is a close correlation between crystal structure of BKBO and its superconducting properties.

In particular, with the emergence of its superconducting behavior at x = 0.35, T_c monotonically decreases with further K doping with the superconductivity remaining entirely until the solubility limit of K at x = 0.6, making a half-dome shaped superconducting phase with potassium concentration [4]. Because of this half-dome superconducting state, it is important to control the stoichiometry of BKBO for obtaining the optimal T_c, since a small deficiency in K concentration from the optimal stoichiometry may destroy the superconducting behavior of BKBO material.

1.2. Oxide thin film growth by using Pulsed laser deposition

Oxide thin films have been grown using numerous techniques, such as pulsed laser deposition (PLD) [8-11], sputtering [12], molecular beam epitaxy [13], and evaporation [14]. Among these growth techniques, PLD is known as a versatile technique for easily fabricating nearly stoichiometric oxide films. For PLD film growth, it is important to control the PLD growth parameters such as laser fluence, substrate temperature, oxygen partial pressure, and post-annealing condition, because they can greatly affect cation and oxygen stoichiometries [15-21] through influencing the plume propagation dynamics.

1.2.1. The effect of background gas pressure on plume propagation dynamics

Background gas pressure have a great effect on the plume propagation in the ablation process. The background gas pressure dependency can be modeled using the physical assumptions. The plume expansion dynamics assumes the plume leading edge as a hemispherical thin layer which receives the counterforce from the background gas while propagating. This plume expansion dynamics can be described as follows [24-26]:

$$\frac{\mathrm{d}}{\mathrm{d}\tau}\left[\left(M_{\mathrm{p}}+M_{\mathrm{g}}(R)\right)u\right]=-F_{\mathrm{p}} \qquad F_p=2\pi R^2 P \qquad \frac{dR}{d\tau}=u$$

where P is the background gas pressure, M_p is the confined plume mass , M_g is the mass of the background gas which previously existed before plume goes by at a distance R, and u is the velocity of the plume hemispherical thin layer.

S. Amoruso, et al [27] has reported the effect of oxygen background gas influence on PLD process of $LaAlO_3$ and $LaGaO_3$. Figure & shows LGO ablation plume at two different time delay after ablated by the laser, with different the oxygen background gas pressure. As shown in the Figure &, high pressure gas up to 1 mbar tends to confine the plume in a parallel direction with respect to target surface, and retard the plume propagation toward the substrate. In this condition, the ablated material has to be diffused into the background gas in order to reach the substrate. On the other hand, the free-expansion dynamics is applied in a low pressure background gas lower than 1 x 10^{-2} mbar. In particular, the difference in plume propagation due to the background gas pressure affects the film stoichiometry, which emphasis on tuning the background gas pressure for obtaining the optimal film properties [27].

1.2.2. The effect of temperature on the film growth

The role of substrate temperature is very crucial in determining the various properties of the films, such as crystallinity, surface morphology, stoichiometry, and electrical transport properties. For example, SrRuO3

film grown at high temperature has been reported to have the improved crystallinity which leads to the conductivity of the films [28]. This is because that the substrate temperature is a main parameter for controlling kinetic energy of the atoms in the film directly. Especially, high substrate temperature evaporates the volatile ablated species, or the lighter elements in the deposited film, resulting in non-stoichiometry.

Moreover, it should be noticed that the substrate temperature can directly affects the plume propagation dynamics. A. Sambri *et al* demonstrated in his paper that the substrate temperature determines the background gas dense profile along the direction of propagation [29]. Therefore, the heated substrate change the growth rate in the ablation process as well as the kinetic energy of atoms on the film surface.

1.2.3. The effect of laser fluence on the element distribution in the propagating plume

The effect of laser fluence in the ablation process is not only for changing the growth rate, but also controlling the stoichiometry of oxide thin films while ablating. In order to avoid non-stoichiometric films, it is important to tune the optimal laser fluence for the stoichiometric composition of oxide films. S. Wicklein *et al*. [16] explained this correlation between film stoichiometry and laser fluence in terms of

incongruent ablation and preferential scattering of lighter ablated elements during the plume propagation toward the substrate.

The initial kinetic energy of the ablated material, and its plume propagation dynamics are defined by the laser fluence. For example, the low laser fluence limits the propagation distance by which the plume travels in the background gas, before the ablated species reaches the substrate. On the other hand, the well-confined plume can propagates in the background gas, reaching the substrate faster than the case of the low fluence. [16]

Even though laser fluence is an essential factor for controlling cation stoichiometry in oxide film growth. [15-17], its effect on superconducting BKBO films has been seldom studied. Especially, a subtle compositional deviation from the stoichiometric BKBO film can result in destroying its superconducting behavior. Therefore, it is necessary to devise comprehensive guidelines for manufacturing high-quality BKBO, by optimizing laser fluence.

1.2.4. The film delamination and spalling

In the film deposition process, film surface usually is at risk of ill-surface problem, which brings about bumpy film surface. The crack occurred at the interface between the film and substrate leads to the subsequent delamination process. There are several reasons of the

interfacial cracks, including the lattice mismatch between the film and substrate, thermal expansion, and oxygen diffusion in / outward the film. Several studies on the film delamination, and spalling has been existed [30-32], which focus on the stress from the compressed or expanded film, and indentation induced compress. In the both condition, the fundamental crack driving force was considered to be related to the buckling on the film surface, having a critical value at which the spalling occurs [30].

Reference

[1] R. J. Cava, B. Batlogg, J. J. Krajewski, R. Farrow, L. W. Rupp, Jr., A. E. White, K. Short, W. F. Peck, and T. Kometani, Nature (London) 332 (1988) 814.

[2] L. F. Mattheiss, E. M. Gyorgy, and D. W. Johnson, Jr., Phys. Rev. B 37 (1988) 3745(R).

[3] D. G. Hinks, B. Daborowski, J. D. Jorgensen, A. W. Mitchell, D. R. Richards, S. Pei, and D. Shi, Nature (London) 333 (1988) 836.

[4] S. Pei, J. D. Jorgensen, B. Dabrowski, D. G. Hinks, D. R. Richards, A. W. Mitchell, J. M. Newsam, S. K. Sinha, D. Vaknin, and A. J. Jacobson, Phys. Rev. B 41 (1990) 4126.

[5] B. A. Baumert, J. Supercond. 8 (1995) 175.

[6] E. V. Antipov, N. R. Khasanova, J. S. Pshirkov, S. N. Putilin, C. Bougerol, O. I. Lebedev, G. Van Tendeloo, A. N. Baranov, Y. W. Park, Curr. Appl. Phys. 2 (2002) 425.

[7] C. Franchini, G. Kresse, and R. Podloucky, Phys. Rev. Lett. 102 (2009) 256402.

[8] B. M. Moon, C. E. Platt, R. A. Schweinfurth, and D. J. Van Harlingen, Appl. Phys. Lett. 59 (1991) 1905.

[9] W.-T. Lin, S.-M. Pan, and K. Chen, Jpn. J. Appl. Phys. 32 (1993) 770.

[10] D. P. Norton, J. D. Budai, B. C. Chakoumakos, and R. Feenstra, Appl. Phys. Lett. 62 (1993) 414.

[11] H. Sato, T. Ido, S. Uchida, S. Tajima, M. Yoshida, K. Tanabe, K. Tatsuhara, and N. Miura, Phys. Rev. B 48 (1993) 6617.

[12] H. Sato, S. Tajima, H. Takagi, and S. Uchida, Nature (London) 338 (1989) 241.

[13] E. S. Hellman, E. H. Hartford and E. M. Gyorgy, Appl. Phys. Lett. 58 (1991) 1335.

[14] Y. Enomoto, T. Murakami, and K. Moriwaki, Jpn. J. Appl. Phys. 28 (1989) L1355.

[15] T. Ohnishi, M. Lippmaa, T. Yamamoto, S. Meguro, and H. Koinuma, Appl. Phys. Lett. 87 (2005) 241919.

[16] D. Kan and Y. Shimakawa, Appl. Phys. Lett. 99 (2011) 081907.

[17] S. Wicklein, A. Sambri, S. Amoruso, X. Wang, R. Bruzzese, A. Koehl, and R. Dittmann, Appl. Phys. Lett. 101 (2012) 131601.

[18] E. Breckenfeld, N. Bronn, J. Karthik, A. R. Damodaran, S. Lee, N. Mason, and L. W. Martin, Phys. Rev. Lett. 110 (2013) 196804.

[19] E. Breckenfeld, R. Wilson, J. Karthik, A. R. Damodaran, D. G. Cahill, and L. W. Martin, Chem. Mater. 24 (2012) 331.

[20] J. N. Zeng, J. K. Low, Z. M. Ren, T. Liew, and Y. F. Lu, Appl. Surf. Sci. 197-198 (2002) 362.

[21] D. Pathak, R. K. Bedi, and D. Kaur, J. Korean Phys. Soc. 56 (2010) 836.

[22] H. Gao, and W. D. Nix, Annu. Rev. Mater. Sci. 29 (1999) 173.

[23] C. Priester, and G. Grenet – Phys. Rev. B, 61 (2000) 16029.

[24] A. Sambri, S. Amoruso, X. Wang, F. Miletto Granozio, and R. Bruzzese, J. Appl. Phys. 104 (2008) 053304.

[25] S. Amoruso, J. Schou, J.G. Lunney, Appl. Phys. A 92 (2008) 907.

[26] R.W.B. Pearse, A.G. Gaydon, The Identification of Molecular Spectra, fourth ed., Chapman and Hall, London, 1984.

[27] S. Amoruso. C. Aruta, P. Aurino, R. Bruzzese, X. Wang, F. M. Granozio, and U. S. Uccio, Appl. Surf. Sci. 258 (2012) 9116.

[28] N. D. Zakharov, K. M. Satyalakshmi, G. Koren, and D. Hesse, J. Mater. Res. 14(11) (1999) 4385.

[29] A. Sambri, S. Amoruso, X. Wang, M. Radovic', F. Miletto Granozio, and R. Bruzzese, Appl. Phys. Lett. 91 (2007) 151501.

[30] A.G. Evans, and J.W. Hutchinson, Int. J. Solids Struct. 20(5) (1984) 455.

[31] W. J. Bottega, and A. Maewal, J. Appl. Mech. 50 (1983) 184.

[32] H. Chai, C. D. Babcock, and W. G. Knauss, Int. J. Solids Struct. 17 (1981) 1069.

2. Experimental Methods

2.1. Pulsed laser deposition

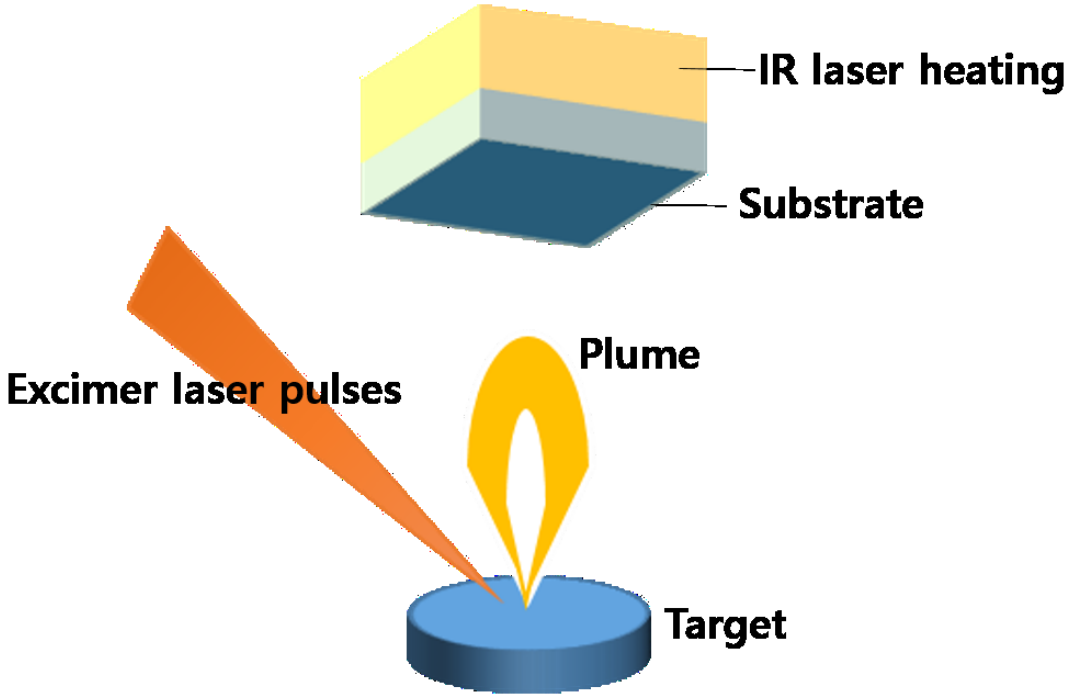

Figure 2.1. A schematic diagram of pulsed laser deposition system

Pulsed laser deposition (PLD) is a growth technique for fabricating stoichiometric oxide films. This technique uses high-power excimer laser by which the laser-absorbed material is conveyed from a target to the substrate. Since PLD is a complex kinetic process occurring in an oxygen environment, PLD growth parameters such as laser fluence, oxygen background partial pressure, and substrate temperature have great effects on film properties [1-7]. Moreover, this technique has an advantage in modulating film parameters like dimensionality and strain [8]. Therefore,

it is necessary to control those PLD parameters for exploring a novel physical properties of solid-state materials.

We used on (001)-oriented $SrTiO_3$ (STO) substrates (Shinkosha) for and PLD (PASCAL; base pressure ~10^{-9} Torr) for a film growth. We also used a K over-doped (Ba:K:Bi = 3:4:5) BKBO target to compensate for possible K deficiency [8-9]. Before deposition, the STO substrates were pre-treated by *in situ* annealing at 950°C in an oxygen partial pressure of 5 × 10^{-6} Torr for 30 min. The target was ablated by a KrF excimer laser (Coherent, wavelength: 248 nm) with a target-to-substrate distance of 5 cm and a repetition rate of 3 Hz. We deposited the BKBO films at 450°C under an oxygen partial pressure of 40 mTorr. Unless otherwise specified, we post-annealed all BKBO films at 400°C in 400-Torr oxygen for 40 min.

2.2. High-resolution X-ray diffractometer

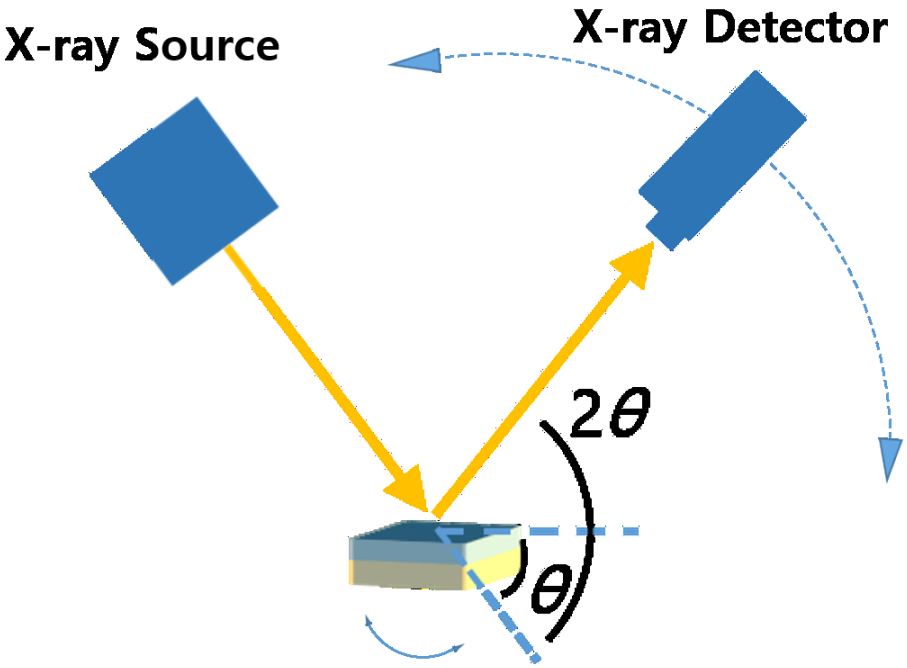

Figure 2.2. A schematic diagram of X-ray diffractometer

X-ray diffractometer (XRD) is a powerful tool to determine the crystal structure of films. In this techniques, an incident x-ray beam is diffracted into various direction by the crystalline atoms. These scattered electromagnetic waves interfere with each other, making diffraction pattern. In pseudo-cubic notation, the diffraction pattern can be understood by the following Bragg model of diffraction.

$$2d_{hkl}sin\theta = n\lambda$$

$$d_{hkl} = \sqrt{a^2/(h^2 + k^2 + l^2)}$$

where *d* is an inter-planar spacing between atomic plains which are described

by three Miller indices (h, k ,l). From this equation, the lattice parameters can be calculated from the position of maximal diffraction.

We investigated the crystal structures using a four-circle, high-resolution X-ray diffractometer (HR-XRD; Bruker) with a Cu-Kα_1 source. We performed 2θ-ω scan, where a sample and a detector move in the same plane, for observing the lattice parameter of films and verifying whether the crystal orientation of the films was well-aligned. In addition, reciprocal space mapping was proceeded for calculating in-plane lattice parameters of the films

2.3. Rutherford backscattering spectrometry

Rutherford backscattering spectrometry (RBS) is used for compositional thin film analysis. RBS technique employs high-energy He^{2+} ions which beamed on the sample. Film composition can be calculated from the amounts and energy of backscattered He^{2+} ions at a particular angle. RBS spectrum provides the useful method to investigate a quantitative information of compositional depth profile for thin films.

In our experiment, we used the Rutherford backscattering (RBS) technique to check the stoichiometry of the BKBO films. By fitting the RBS spectra using a program for the simulation of backscattering spectra for ion beam analysis (SIMNRA; IPP), we were able to obtain the relative ratio of elements Ba, K, and Bi.

2.4. Atomic force microscopy

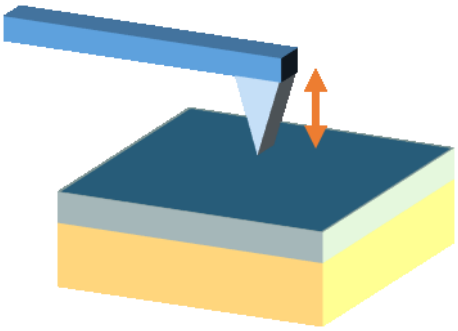

Figure 2.3. A schematic diagram of Atomic force microscopy

Atomic force microscopy (AFM) is an effective equipment for studying film surface morphology. It can provide a high-resolution three dimensional topological image of the sample surface using the force applied on the probe. We investigate film surface morphology with an Asylum Instrument Cypher AFM. The image process is done with Gwyddion software package.

2.5. Electrical transport measurement setup

To investigate *dc* transport properties, we used a custom-made closed-cycle refrigerator in four-probe geometry with carbon paste electrodes. Typical sample dimensions were 1.5 × 5 mm^2. We also used a stylus profiler, to measure film thickness. The thickness of each sample was approximately 100 nm.

References

[1] T. Ohnishi, M. Lippmaa, T. Yamamoto, S. Meguro, and H. Koinuma, Appl. Phys. Lett. 87 (2005) 241919.

[2] D. Kan and Y. Shimakawa, Appl. Phys. Lett. 99 (2011) 081907.

[3] S. Wicklein, A. Sambri, S. Amoruso, X. Wang, R. Bruzzese, A. Koehl, and R. Dittmann, Appl. Phys. Lett. 101 (2012) 131601.

[4] E. Breckenfeld, N. Bronn, J. Karthik, A. R. Damodaran, S. Lee, N. Mason, and L. W. Martin, Phys. Rev. Lett. 110 (2013) 196804.

[5] E. Breckenfeld, R. Wilson, J. Karthik, A. R. Damodaran, D. G. Cahill, and L. W. Martin, Chem. Mater. 24 (2012) 331.

[6] J. N. Zeng, J. K. Low, Z. M. Ren, T. Liew, and Y. F. Lu, Appl. Surf. Sci. 197-198 (2002) 362.

[7] D. Pathak, R. K. Bedi, and D. Kaur, J. Korean Phys. Soc. 56 (2010) 836

[8] H.Y. Hwang, Y. Iwasa, M. Kawasaki, B. Keimer, N. Nagaosa and Y. Tokura, Nat. Mat. 11 (2012) 103

3. Ablation laser fluence as an effective parameter to control superconductivity in $Ba_{1-x}K_xBiO_3$ films*

3.1. Structural change with variation of laser fluence in HR-XRD

In order to investigate the effect of ablation laser fluence on properties of BKBO film, we varied the laser fluence from 0.58 to 2.18 J/cm^2 by using a variable attenuator, while a laser spot size was fixed at 1.5 × 1.5 mm^2. Figure 3.1.(a) and 3.1.(b) show X-ray diffraction (XRD) θ-2θ scans of BKBO films grown with various laser fluence values. We observed clear (001) and (002) Bragg reflections of BKBO and STO. Since there are no reflections from other planes, the crystallographic directions of the film were well aligned with those of the substrate. Reciprocal space mapping (RSM) image in Figure 3.2.(a) for a representative sample grown at 1.05 J/cm^2 around the (103) STO reflection shows that the film became relaxed due to the large lattice mismatch between STO (a = 3.905 Å) and bulk BKBO ($a \approx$ 4.28* Å).

We found that laser fluence had a significant effect on the structural parameters of the BKBO films. In Figure 3.1.(b), the enlarged pattern of (002) film reflections shows a systematic shift of the (002) reflections to higher 2θ angles, as the laser fluence increase. This observed 2θ shift means that c_{film} decreases with an increase in the laser fluence. Figure

* The content and figures in this chapter was accepted to be published in H. Lee *et al, SI: Oxide Heterostructure*, Curr. Appl. Phys. 2017 [1]

3.2.(b) summarizes the values of a_{film} and c_{film} obtained from the RSM and (002) BKBO reflections in the XRD θ-2θ scan, respectively. Both a_{film} and c_{film} decreased as we increase the laser fluence, which resembles the bulk structural phase diagram of BKBO, where lattice parameters decrease in response to increasing the K concentration [2].

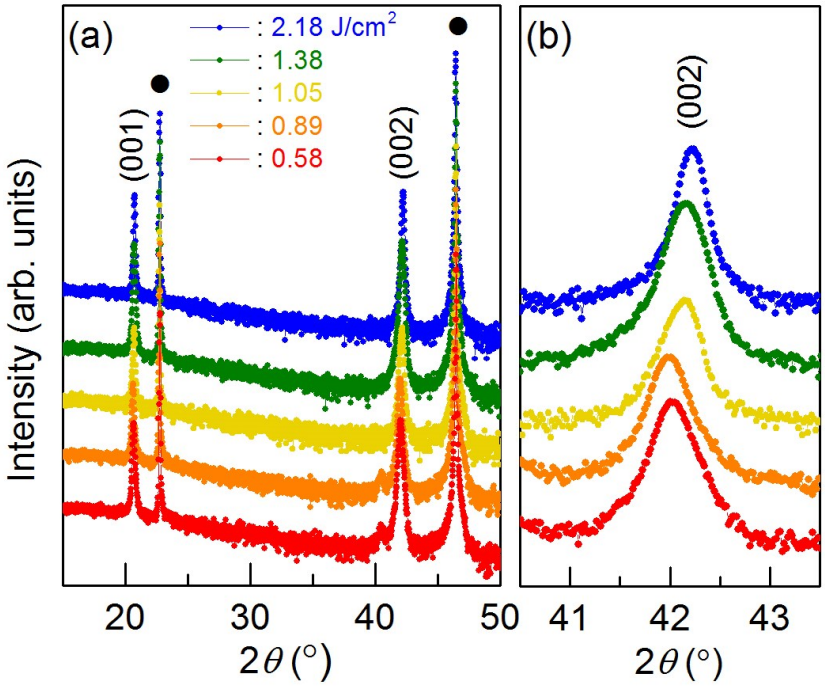

Figure 3.1. (a) X-ray diffraction (XRD) θ-2θ scans for various laser fluences. The circle symbols indicate XRD peaks of (001) and (002) STO substrates. (b) Enlarged (002) Bragg reflection patterns. The pseudo-cubic notation was used for all BKBO reflections discussed in this paper [1].

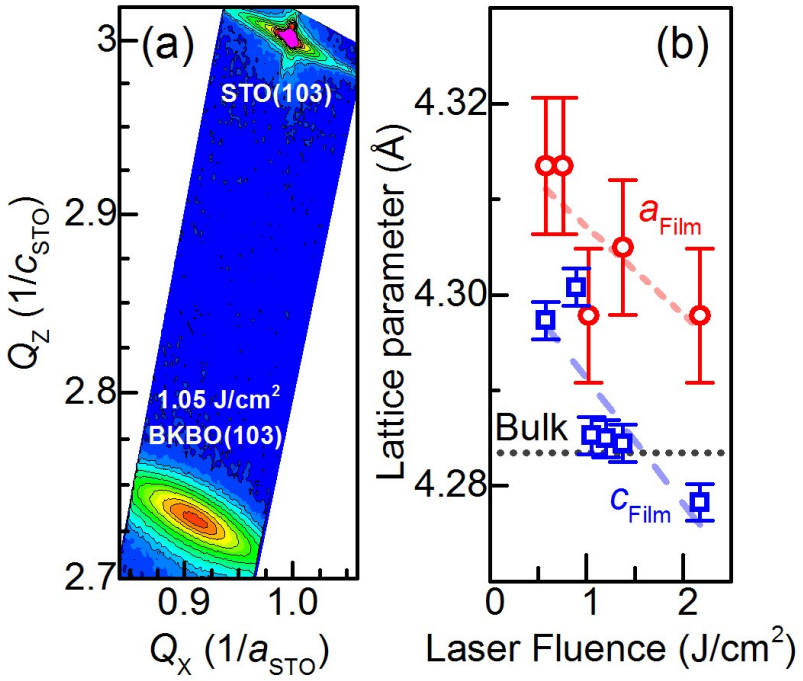

Figure 3.2. (a) A reciprocal space map (RSM) around the (103) STO Bragg reflection, for a BKBO film grown with a laser fluence of 1.05 J/cm^2. (b) The lattice parameters of BKBO films grown with various laser fluences. We included error bars to reflect the broadness of the XRD peaks. The horizontal black dotted line indicates the lattice parameter of the bulk cubic BKBO, a_{BKBO} = 4.283 Å [1].

3.2. Cation composition which is highly dependent on laser fluence

We experimentally determined the chemical stoichiometry of our BKBO films by using RBS technique. Figure 3.3.(a) shows the RBS spectra for a film grown at 1.05 J/cm^2, from which relative concentrations of Ba, K, and Bi were determined. The oxygen spectrum was not analyzed due to complications arising from the substrate oxygen. Large variations existed in the cation compositions that are dependent on laser fluence, as shown in Figure 3.3.(b). The RBS results demonstrate that the cation composition of PLD-grown BKBO films was indeed highly dependent on laser fluence. As the laser fluence increased from 0.59 to 2.31 J/cm^2, the K concentration increased from 0.14 to 0.3, and the Bi concentration decreased from 0.55 to 0.4. Stoichiometric BKBO films close to the optimally doped bulk (Ba:K:Bi = 0.6:0.4:1) were fabricated between laser fluences of 1.05 and 1.38 J/cm^2.

This correlation between laser fluence and film stoichiometry can be explained in terms of preferential scattering of lighter ablated elements during the plume propagation into the substrate [3]. In other words, a lighter element (K in our experiment) tends to scatter more than other heavier ablated elements within the background gas. In particular, laser fluence determines its initial velocity and the mass of the plume, which determine the plume propagation within the oxygen background gas [4]. For example, the plume is too slow to reach the substrate at low laser fluence. In this conditions, ablated species must diffuse through the background gas to arrive

at the substrate. Because the lighter element tends to scatter over larger angles compared with the heavier elements [3], only a relatively small portion of the lighter element arrives at the substrate. This explains why the BKBO films grown at low laser fluence have small K concentrations. As laser fluence increases, it becomes easier for K ions to reach the substrate, increasing the K concentration of the BKBO films. The decrease in the relative Bi ratio can be understood in terms of the relative increase of K and Ba, via the same mechanism. With regards to the low Bi concentrations at high laser fluence, it should be noted that we could not find any indications of impurity phases from Bi deficiency in the X-ray diffraction pattern [Figure 3.1.(a)]. This may imply that the impurity phases originating from Bi deficiency are too small to be detected, or that they are amorphous.

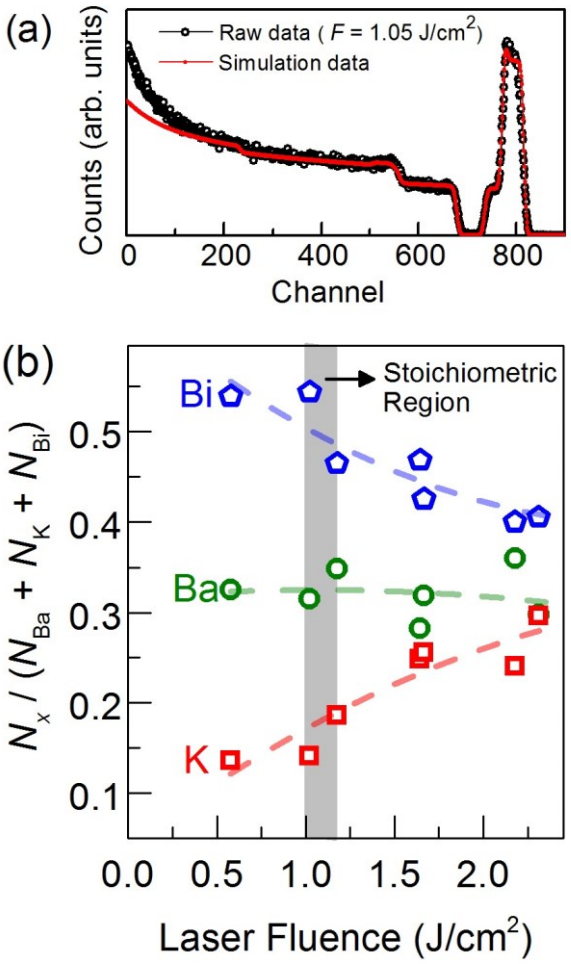

Figure 3.3. (a) Chemical element analysis of BKBO films by Rutherford backscattering spectroscopy (RBS). The counts of elements Ba, K, and Bi are calculated by fitting the RBS data. (b) Relative concentrations of Ba, K, and Bi elements as a function of laser fluence. A relative concentration is defined as the ratio of a certain element to the sum of the three elements: Ba, K, and Bi. The gray shaded area indicates a regime of stoichiometric BKBO films, in which the bulk BKBO exhibits the highest superconducting transition temperature, T_c = 31 K. [1]

3.3. A variation of T_c with laser fluence observed by resistivity measurement

Electrical transport measurements showed a variation of T_c with laser fluence, which indicates that the stoichiometry controlled by laser fluence has a strong influence on superconductivity in BKBO films. All BKBO films grown within the range of 0.58 to 2.18 J/cm^2 exhibited a superconducting transition, as shown in Figure 3.4.(a). Films grown using a laser fluence of less than 0.58 J/cm^2 were insulating (R_{300K} = 1 MΩ/sq.) rather than superconducting. This can be attributed to the low K concentration of the films, consistent with the RBS results [Figure 3.3.(b)].

We confirmed the Meissner effect of the superconducting BKBO film, as shown in Figure 3.4.(b). Under 20 K, the diamagnetism of the representative film was continuously intensified down to 3 K. Curiously, we observed disagreement between T_c in the resistivity and that in the magnetic moment. We consider the T_c difference to be resulted from the inhomogeneity in the film. Since the magnetic property measurement system is sensitive to the bulk property of the film, the disproportion in the film stoichiometry can degrade the superconducting transition, broadening the superconducting transition range, or decrease T_c in the magnetic moment measurement, while a linear portion of superconducting film results the zero resistance value in the resistivity measurement.

Figure 3.4.(c) summarizes the experimental values of T_c and R_{30K}, where we defined R as the sheet resistance, R_{30K} as the sheet resistance of

the normal state at 30 K, and T_c as the mid-point of the superconducting transition. As expected, the most stoichiometric BKBO films achieved the maximum T_c value of 24.5 ± 0.5 K, as well as the minimum R_{30K} value of about 45 Ω/sq. The decrease of T_c at high laser fluence resembles the previously reported BKBO phase diagram, in which T_c also decreased in the K-overdoped regime [2]. Likewise, considering the fact that high K concentrations were obtained in the BKBO films grown at high laser fluence, the decrease of T_c at high laser fluence can be explained by the increase in K concentration.

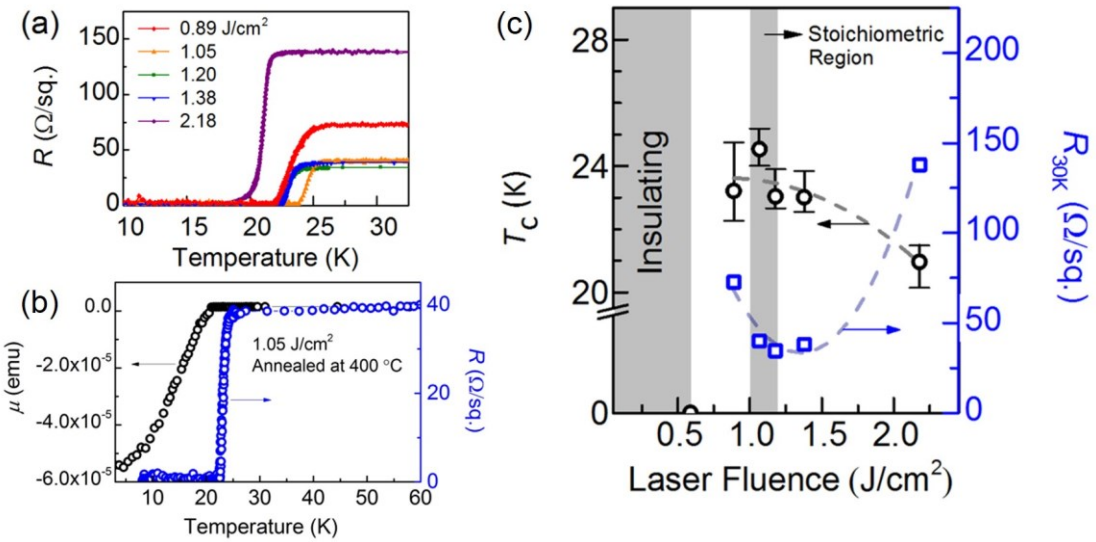

Figure 3.4. (a) The sheet resistance (R) of the BKBO films as a function of the film temperature for various laser fluences. (b) The magnetic moment of a representative film (grown at the laser fluence of 1.05 J/cm^2 and annealing temperature of 400 °C. (c) Laser fluence dependence of both the superconducting transition temperature T_c and the sheet resistance R_{30K} (R measured at 30 K). Films that were grown using a laser fluence of less than 0.58 J/cm^2 were insulating rather than superconducting. We included error bars to reflect the width of T_c, whose range extended from 10% to 90% of R_{30K}. [1]

However, the T_c of our stoichiometric BKBO films were not as large as that of the bulk counterpart (i.e., ~31 K). This means that in the BKBO films, there are some other factors that degrade T_c, in addition to the cation non-stoichiometry. In fact, this discrepancy in T_c was an unsolved problem in early BKBO film studies [5], where T_c values of BKBO films were smaller than that of bulk BKBO by at least several degrees [6-12].

3.4. Compensation of oxygen vacancies by post-annealing procedure

Regarding this difference in T_c, we first comment on the oxygen stoichiometry in our BKBO films, since the oxygen stoichiometry has a critical influence on the superconducting properties of BKBO. The oxygen deficiency of BKBO dopes excess electrons that compensate holes in the valence band as well as increase the Bi-O bond distance, resulting in insulating behavior [13-14]. In fact, suppression of the superconducting transition of BKBO has been reported above a certain oxygen vacancy content ($\delta = 0.31$) [14]. Therefore, we attempted to eliminate oxygen deficiency in the BKBO films using post-annealing in oxygen gas.

Specifically, we were able to optimize the oxygen stoichiometry in the BKBO films by varying the post-annealing temperature [7, 9, 13, 15]. The films that were subject to post-annealing in oxygen within the temperature range of 400 °C to 500 °C clearly exhibited superconducting properties, as shown in Figure 3.5.(a). All films were post-annealed in 400-Torr oxygen for 40 min. Figure 3.5.(b) shows T_c and R_{30K} as functions of the post-annealing temperature. Low post-annealing temperatures did not fully fill oxygen vacancies in the BKBO films: the films post-annealed below 350 °C were insulating. The metallic behavior of BKBO films only appeared when using post-annealing temperatures above 400 °C. However, post-annealing at even higher temperatures did not further reduce the resistivity or increase T_c, implying that the cation stoichiometry may have deviated from that of the as-grown films. The optimal post-annealing

temperature range was from 400 °C to 450°C. This is the range of temperatures over which the highest T_c and the lowest resistivity were obtained.

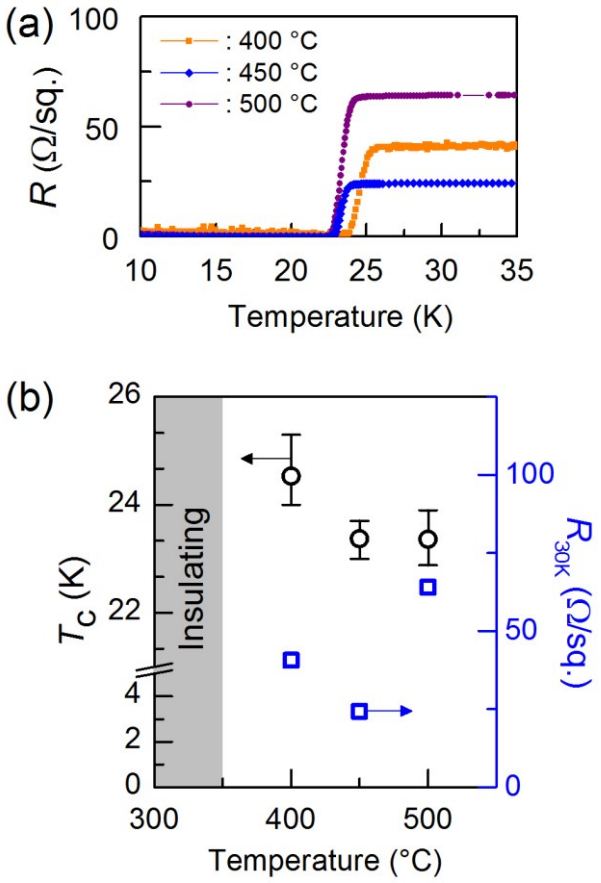

Figure 3.5. (a) The sheet resistance (R) of BKBO films, as a function of the film temperature for various annealing temperatures. (b) Annealing temperature dependence of both the superconducting transition temperature T_c and the sheet resistance R_{30K} (R measured at 30 K). We confirmed the insulating behavior of BKBO films post-annealed below 350°C. The BKBO films post-annealed at 400°C exhibited the highest T_c, although the smallest R_{30K} was obtained in films post-annealed at 450°C. For the data set corresponding to Figures 5(a) and (b), all samples were grown at a laser fluence of 1.05 J/cm^2 [1].

Apart from considerations of oxygen vacancy, we speculate that the discrepancy in T_c between BKBO films and the bulk may be due to the crystallographic defects in the BKBO films. In other words, interstitial and/or anti-site defects, originating from the low growth temperature (~450 °C), may degrade T_c of the BKBO films. In fact, all BKBO films had large full-width half-maximum (FWMH) values regarding the (002) reflection rocking curve of 1.48 deg. in XRD measurement, indicating the existence of an inferior structural phase within the BKBO films. It may be possible to deal with these lattice imperfections in the BKBO films by increasing the growth or annealing temperatures. However, volatile elements such as K in our experiment are easily evaporated, and superconducting behavior can disappear when the growth temperatures are above 500 °C [6, 8]. Thus, it will be necessary to find an alternative method to enhance the T_c of BKBO films, such that neither the crystallinity nor the sufficiently high K concentration of the BKBO films is compromised. For future research on BKBO films, we suggest the introduction of a repeated temperature modulation (RTM) technique [16] that will periodically repeat the growth sequences via rapid switching between film deposition at low temperature and film crystallization at high temperature.

Reference

[1] H. Lee, M. Kim, O. B. Korneta, S. Lee, T. W. Noh, Curr. Appl. Phys. (2017, accepted)

[2] S. Pei, J. D. Jorgensen, B. Dabrowski, D. G. Hinks, D. R. Richards, A. W. Mitchell, J. M. Newsam, S. K. Sinha, D. Vaknin, and A. J. Jacobson, Phys. Rev. B 41 (1990) 4126.

[3] S. Wicklein, A. Sambri, S. Amoruso, X. Wang, R. Bruzzese, A. Koehl, and R. Dittmann, Appl. Phys. Lett. 101 (2012) 131601.

[4] G. Koster, M. Huijben, and G. Rijnders, Epitaxial Growth of Complex Metal Oxides, Elsevier, 2015, pp. 235.

[5] E. S. Hellman and E. H. Hartford Jr., Physica C 190 (1991) 31.

[6] B. M. Moon, C. E. Platt, R. A. Schweinfurth, and D. J. Van Harlingen, Appl. Phys. Lett. 59 (1991) 1905.

[7] W.-T. Lin, S.-M. Pan, and K. Chen, Jpn. J. Appl. Phys. 32 (1993) 770.

[8] D. P. Norton, J. D. Budai, B. C. Chakoumakos, and R. Feenstra, Appl. Phys. Lett. 62 (1993) 414.

[9] H. Sato, T. Ido, S. Uchida, S. Tajima, M. Yoshida, K. Tanabe, K. Tatsuhara, and N. Miura, Phys. Rev. B 48 (1993) 6617.

[10] H. Sato, S. Tajima, H. Takagi, and S. Uchida, Nature (London) 338 (1989) 241.

[11] E. S. Hellman, E. H. Hartford and E. M. Gyorgy, Appl. Phys. Lett. 58 (1991) 1335.

[12] Y. Enomoto, T. Murakami, and K. Moriwaki, Jpn. J. Appl. Phys. 28 (1989) L1355.

[13] W. D. Mosley, J. W. Dykes, P. Klavins, R. N. Shelton, P. A. Sterne, and R. H. Howell, Phys. Rev. B 48 (1993) 611.

[14] K. Ueki, A. Tokiwa, M. Kikuchil, T. Suzuki, M. Nagoshi, R. Suzuki, N. Kobayashi, and Y. Syono, Advances in Superconductivity II, Springer, Japan, 1990, pp. 489-492.

[15] W. S. Choi, D. W. Jeong, S. Y. Jang, Z. Marton, S. S. A. Seo, H. N. Lee, and Y. S. Lee, J. Korean Phys. Soc. 58. (2011) 569

[16] A. Tsukazaki, A. Ohtomo, T. Onuma, M. Ohtani, T. Makino, M. Sumiya, K. Ohtani, S. F. Chichibu, S. Fuke, Y. Segawa, H. Ohno, H. Koinuma, and M. Kawasaki, Nat. Mater, 4 (2005) 42.

4. Epitaxial growth of BKBO films on various buffer layer for a strain control

4.1. BKBO film with a BBO buffer layer

An un-doped perovskite oxide $BaBiO_3$ (BBO) has a cubic structure with a lattice parameter of 4.38 Å, which corresponds to +2.4 % mismatch with that of bulk BKBO. In order to reduce lattice mismatch, therefore, we used BBO buffer layer with 15 nm thickness on SrTiO3 substrate. We deposited BBO buffer layer onto STO(001) substrate of 500 °C in 100 mTorr oxygen background gas, with a laser fluence of 0.5 J/cm^2. At this condition, a deposition of 500 pulses corresponded to the thickness of 15 nm. Even though BBO has a large lattice mismatch of +12.2 % with the substrate, we obtained the BBO film with a small roughness of 0.326 nm, and step structure was clearly seen, as shown in Figure 4.1.(a), while rough BKBO surface was observed as shown in Figure 4.1.(b).

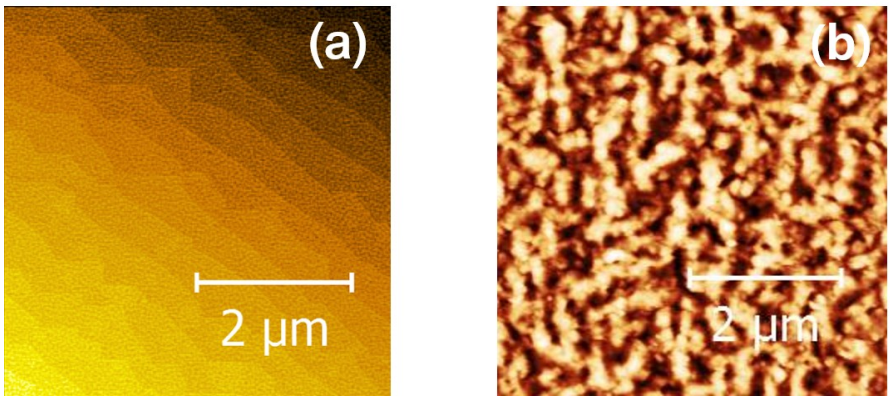

Figure 4.1. AFM Image of BBO/STO and BKBO/STO. (a) BBO/STO with thickness of 22 nm, and roughness of 0.326 nm on STO substrates. (b) BKBO/STO with thickness of 100 nm with a rough surface over roughness of 10 nm.

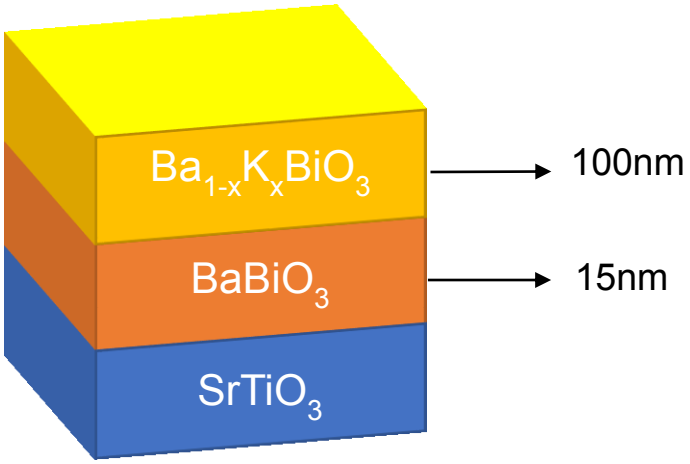

Figure 4.2. Schematic diagram of BKBO film with BBO buffer layer on STO substrate.

After deposition of BBO buffer layer, we deposited BKBO film on the buffer layer [Figure 4.2.], with the same BKBO growth condition used in section 3. We examined the film epitaxy by obtaining reciprocal space mapping image as shown in Figure 4.3. From the result, the BKBO/BBO film was mostly relaxed, while there is a small coincidence in in-plane lattice parameters between BKBO and BBO.

Figure 4.4. is an AFM image of surface on BKBO/STO and BKBO/BBO/STO. Interestingly, a mosaic pattern with small rectangles was observed on the BKBO/BBO film, which was not seen in BKBO/STO as shown in Figure 4.1.(a). This rectangular pattern is regarded as a kind of crack which was generated during the film deposition process [1]. However, we could not remove the crack pattern even though we increase the time for heating and cooling the film, which means that it may not originate from the sudden temperature change in the film deposition process.

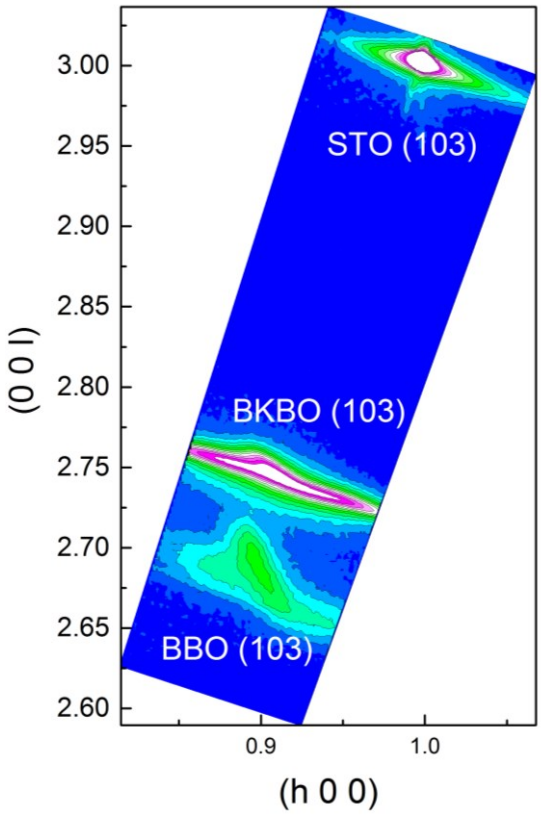

Figure 4.3. A reciprocal space map (RSM) around the (103) STO Bragg reflection for BKBO film with BBO buffer layer

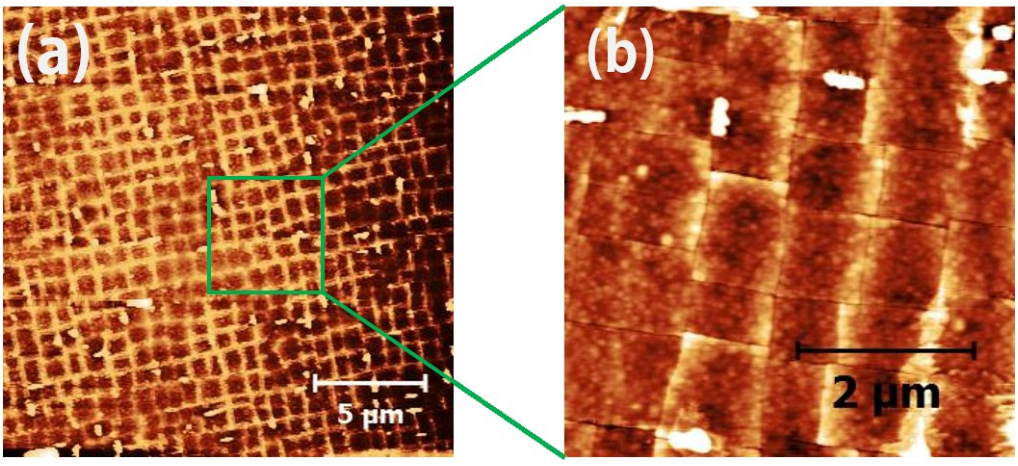

Figure 4.4. AFM Image of BKBO/STO and BKBO/BBO/STO (20um x 20um or 5um x 5um)

Instead, this crack can be explained as the film delamination [1-4]. A BKBO lattice constant, about 4.28 Å, is larger than that of BBO buffer layer, 4.34 Å. Therefore, the tensile strain was applied to the BKBO film, causing the delamination on the film. It is interesting that even a relatively small mismatch (1.4%) brought about the film delamination, while there were no such rectangular cracks on BKBO films without buffer layer as shown in Figure 4.1.(b). These cracks on BKBO film, unfortunately, made it hard to measure the film resistance, making the resistance value very large.

In addition to the interesting crack on the film surface, the BKBO/BBO film has a better crystal quality than those of the films without the buffer layer. Figure 4.5 shows the (002) reflection rocking curve corresponding to BKBO layer. It is interesting that the (002) reflection rocking curve for BKBO with BBO buffer layer consists of two curves. We designates the broad one as un-strained BKBO film, since the same broad rocking curve has been observed in BKBO film without buffer layer, and the sharp one as strained BKBO film. The FWHM of (002) rocking curve for the sharp BKBO film is less than one third of that for the BKBO film without a buffer layer. This decline in FWHM of the strained film rocking curve means an increase in the portion of the identical crystal structure in the film, while a large FWHM of the film rocking curve manifests that each unit-cell structure is not mostly identical. These results put an emphasis on a small lattice mismatch between the film and the

bottom layer for the better surface and crystal quality [2-4].

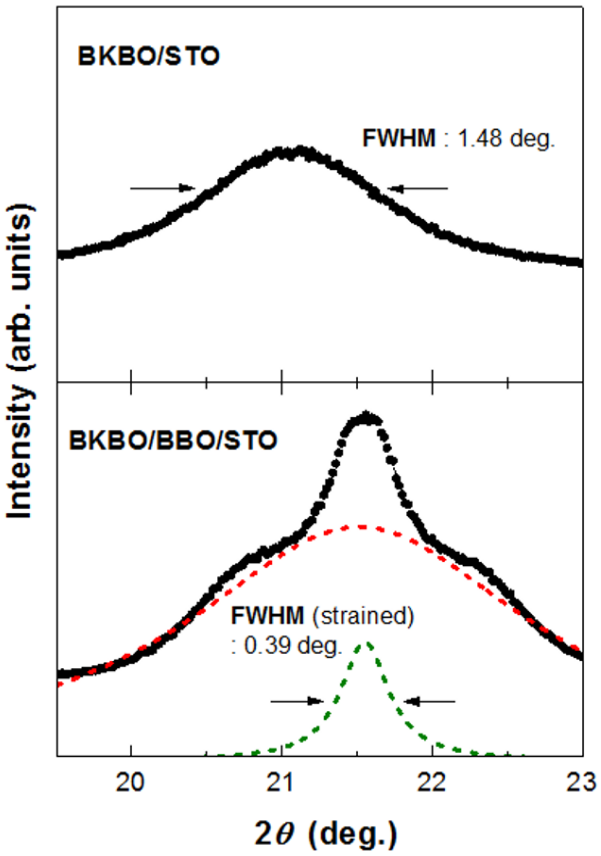

Figure 4.5. The (002) reflection rocking curve of BKBO/STO and BKBO/BBO/STO. BKBO with the double buffer layer has overlapped rocking curves, which corresponds each to strained and unstrained BKBO film. Strained BKBO film has the smaller FWHM value than that of unstrained BKBO film.

4.2. BKBO film with BCO/BZO double buffer layer

An un-doped perovskite oxide $BaZrO_3$ (BZO) has a cubic structure with a lattice parameter of 4.19 Å, which corresponds to -2.1% mismatch with that of bulk BKBO. Like the case of BBO buffer layer, we investigated whether the compressive strain effect of BaZrO3 buffer layer (4.19 Å) can be applied to the BKBO film.

We deposited BZO buffer layer onto STO (001) substrate of 700 °C in 100 mTorr oxygen background gas, with a laser fluence of 1 J/cm^2. At this condition, we found that a deposition of 1000 pulses corresponding to the thickness of 24 nm. After the deposition of 24 nm BZO buffer layer on the substrate, we cooled down temperature to 450 °C and decrease the background oxygen pressure down to 40 mTorr in order to deposit the BKBO film. Likewise the previous experiments, post-annealing procedure under 400 Torr oxygen gas was followed. However, from RSM data, as shown in Figure 4.7.(a), we unfortunately observed the fully relaxed BKBO film on BZO buffer layer. Instead, we found the other buffer layer that could be used for applying strain on BKBO film.

Orthorhombic perovskite $BaCeO_3$ (BCO) has a pseudo-cubic lattice constant of 4.39 Å, which corresponds to +2.5 % mismatch with that of bulk BKBO. We tried to deposit BCO buffer layer on STO (001) substrate. However, the deposited BCO layer has an amorphous phase in XRD measurement. Therefore, we used BaCeO3 / BaZrO3 double buffer layer

[5], since we could not deposit single crystalline BCO buffer layer alone on STO (001) substrate. In the same with BZO deposition, we found that a deposition of 1000 pulses corresponding to the thickness of 24 nm. After BCO deposition, we deposited the BKBO films onto BCO/BZO double buffer layer with the same BKBO growth condition [Figure 4.6.].

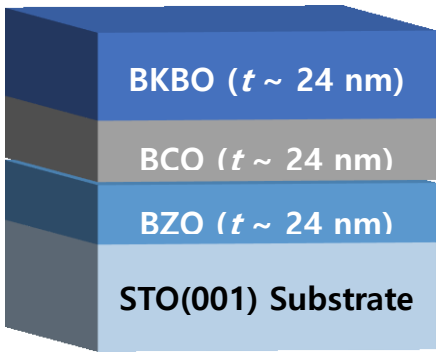

Figure 4.6. Schematic diagram of BKBO with BCO/BZO double buffer layer

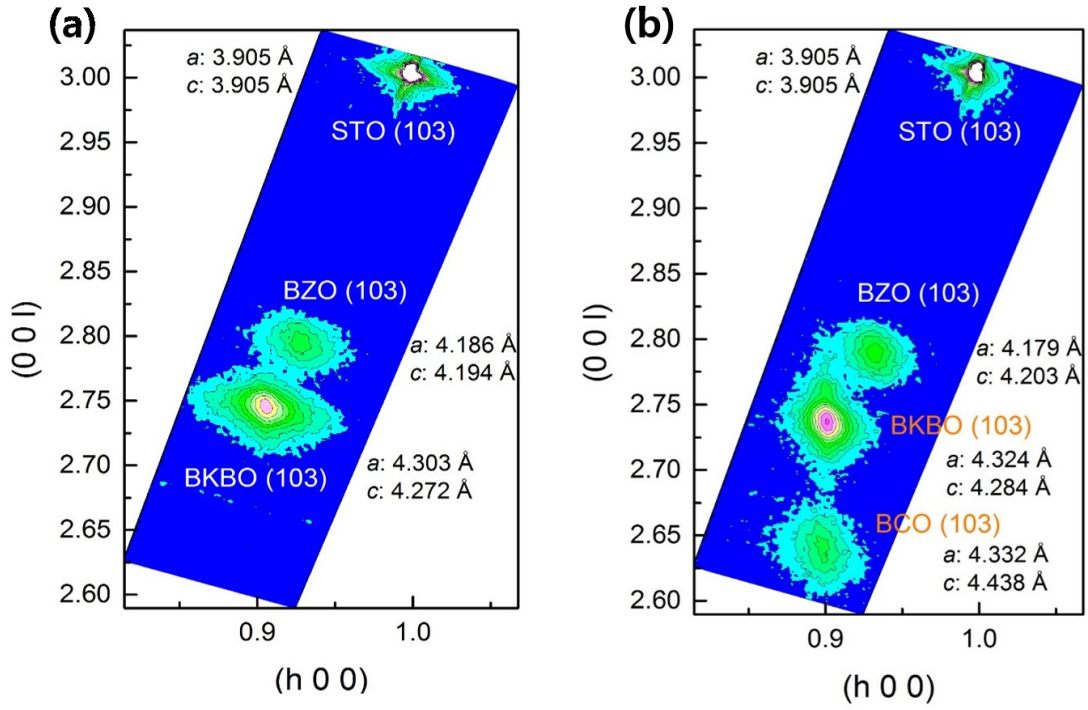

Figure 4.7. Reciprocal space maps (RSM) around the (103) STO Bragg reflection for (a) BKBO/BZO/STO and (b) BKBO/BCO/BZO/STO.

From RSM data, as shown in Figure 4.7.(b), we found the epitaxial growth of BKBO film on the BCO/BZO double buffer layer showing agreement in in-plane lattice parameter with an error of +0.18 %. Comparing to the bulk BKBO, the tensile strain of 1 % was applied to the BKBO film with BCO/BZO double buffer layer.

This epitaxial growth of BKBO film onto the BCO/BZO double buffer layer has indeed impacts on the crystal quality of the BKBO films. Figure 4.8.(b) shows FWHM of (002) reflection rocking curve, which is 200 times smaller than that of the BKBO film without buffer layer, shown in Figure 4.8.(a). It demonstrates that the BKBO film epitaxially grown on BCO/BZO double buffer layer has improved crystal quality, which was not

possible to obtain in the BKBO films without buffer layers. However, contrast to the BKBO/BBO hetero-structure, we could not find a particular improvement on the surface morphology of the BKBO film as shown in Figure 4.8.(c), which compares to the case of BKBO/BBO hetero-structure.

Nevertheless, this result emphasis on the role of buffer layer in improving crystal quality of BKBO films. It suggest the possibility to reduce the crystallographic defects in BKBO films, which could harm the superconducting behavior of BKBO films, as discussed in section 3, using buffer layers. Therefore, a detail investigation on the effect of buffer layer on the superconducting transition temperature T_c, which brings about the improvement on crystal quality of BKBO films, would be recommendable for a future research.

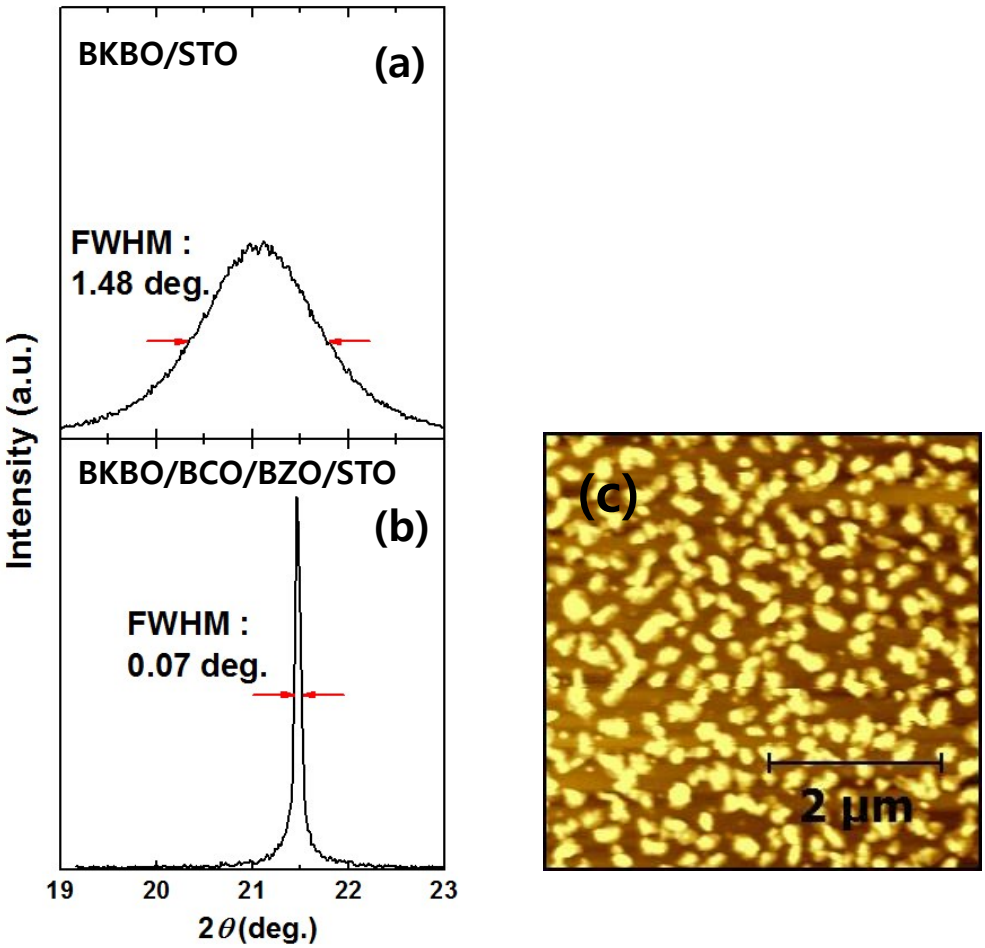

Figure 4.8. The (002) reflection of BKBO rocking curve for (a) BKBO without buffer layer and (b) with BCO/BZO double buffer layer. (c) AFM surface image of BKBO film with BCO/BZO double buffer layer

Reference

[1] E. S. Hellman, E. H. Hartford, and E. M. Gyorgy, Appl. Phys. Lett., 58(12) (1991) 1335.

[2] H. Gao, and W. D. Nix, Annu. Rev. Mater. Sci. 29 (1999) 173.

[3] C. Priester, and G. Grenet, Phys. Rev. B, 61 (2000) 16029.

[4] R. S. Telyatnik, A. V. Osipov, and S. A. Kukushkin, Phys. Solid State, 57(1) (2015) 162.

[5] H. G. Lee, Y. Kim, S. W. Hwang, G. Kim, T. D. Kang, M. Kim, M. Kim, and T. W. Noh. Appl. Phys. Lett. Mate. APL Mat. 4(12) (2016) 121101.

5. Conclusions

We investigated *in situ* growth control of superconducting properties of BKBO films, by varying growth parameters using pulsed laser deposition. We revealed the contraction of lattice parameters in BKBO films with an increase of laser fluence, which could be explained by an increase of K concentration. The sensitive variation of K concentration with laser fluence allowed us to precisely control T_c of BKBO films. The maximum $T_c \approx 24.5$ K was obtained in the films with the stoichiometry mostly similar to the optimally doped bulk BKBO. The degradation of T_c to the bulk counterpart may be originated from the crystallographic disorders in the BKBO films.

In addition, a well tensile-strained BKBO film with a $BaCeO_3$ / $BaZrO_3$ double buffer layer had sharp full-width-half-maximum (FWHM) of the (002) reflection rocking curve of the films in HR-XRD measurement, which emphasis on the role of the buffer layer for the film surface quality.

Our works will not only provide useful guidance for the synthesis of high-quality of high-T_c superconducting BKBO films, but also support the study on the effectiveness of growth parameters including laser fluence for emerging optimized superconducting properties in various PLD-grown complex oxide thin films

펄스레이저 증착에서 레이저 세기속 조절과 완충 층 사용을 통한 $Ba_{1-x}K_xBiO_3$ 박막의 구조적 또는 전기적 물성 연구

이 연구에서는 Pulsed laser deposition (PLD) 장치를 이용하여 BKBO 박막을 증착할 때 박막의 성장 조건이 BKBO 박막의 초전도 특성에 어떠한 영향을 미치는지를 조사한다. 특히 레이저 에너지 속(Laser Fluence)을 달라짐에 따라 박막의 양이온 조성비가 변화하는 것을 발견하였으며 그를 통해 BKBO 박막의 T_c를 조절할 수 있었다. 이 실험 결과에서 박막이 최적의 조성비, 즉 벌크에서 가장 높은 T_c가 관찰되는 조성비에서 박막 또한 가장 높은 T_c가 관측되었다. 이러한 우리의 결과가 고품질의 BKBO 박막의 최적의 합성 방법 연구뿐만 아니라 PLD를 이용한 초전도 산화물 박막 증착에서 초전도 현상 발현에 관한 레이저 에너지 속의 효과 연구에도 큰 도움을 줄 것이라 기대한다.

또한, $BaBiO_3$ 완충 층을 사용하여 부분적으로 인장력을 받은 BKBO 박막과 $BaCeO_3$ / $BaZrO_3$ 이중 완층 층을 사용하여 완전하게 인장력을 받은 BKBO 박막을 이번 연구를 통해 제작하였다. 두 경우 모두, X-ray 회절계를 이용한 Rocking curve 측정 실험에서 BKBO 박막의 (002) 방향의 작은 반치전폭 값을 관측하였다. 이러한 결과는 다양한 완충 층의 사용이 BKBO 박막의 결정학상의 결함을 줄일 수 있는 가능성을 보여준다.